Journal of Power Sources 204 (2012) 1–13

Contents lists available at SciVerse ScienceDirect

Journal of Power Sources

journal homepage: www.elsevier.com/locate/jpowsour

Electrooxidation of acetaldehyde on a carbon supported Pt catalyst at elevated temperature/pressure: An on-line differential electrochemical mass spectrometry study

S. Sun, M. Heinen [1], Z. Jusys, R.J. Behm *

Institute of Surface Chemistry and Catalysis, Ulm University, D-89069 Ulm, Germany

ARTICLE INFO

Article history:
Received 23 July 2011
Received in revised form 9 December 2011
Accepted 10 December 2011
Available online 19 December 2011

Keywords:
Acetaldehyde oxidation
High temperature DEMS
CO_2 current efficiency
Acetic acid oxidation
Apparent activation energy, Supported Pt catalyst

ABSTRACT

The electrooxidation of acetaldehyde on a Pt/Vulcan catalyst was investigated over a wide range of temperatures (23–100 °C) in a flow cell under controlled transport conditions, employing high temperature/high pressure (3 bar overpressure) on-line differential electrochemical mass spectrometry (DEMS). Potentiodynamic and potentiostatic measurements of the Faradaic current and of the CO_2 formation rate reveal that complete oxidation to CO_2 prevails only at higher temperatures and lower potentials, with ~80%/40% current efficiency for CO_2 formation at 0.5 V/0.6 V in 0.1 M solution and at 100 °C, in contrast to a few percent at room temperature. Oxidation to acetic increases at higher potential. The increase of the CO_2 current efficiency with temperature is reflected by a higher apparent activation barrier for complete oxidation to CO_2 (39 ± 2 kJ mol^{-1} at 0.6 V, 0.1 M) compared to that of the overall acetaldehyde oxidation reaction given by the Faradaic current (32 ± 2 kJ mol^{-1}) and that for oxidation to acetic acid (27 ± 3 kJ mol^{-1}). Analogous measurements on the electrooxidation of acetic acid show very low reactivities even at 100 °C, and a high apparent activation energy (173 ± 6 kJ mol^{-1}). The importance of fuel cell relevant reaction and mass transport conditions in model studies is discussed.

1. Introduction

Since acetaldehyde and acetic acid are reaction side products and possibly also reaction intermediates of the ethanol oxidation reaction [1–6], their interaction with metal electrode surfaces and supported catalysts is highly relevant for understanding the reaction characteristics in direct ethanol fuel cells (DEFCs) [7–12]. Accordingly, these reactions have been studied on a number of electrodes and supported catalysts [1,5,6,13–20]. Different from reaction conditions in a fuel cell, however, most of these studies were performed under ill-defined transport conditions and at room temperature. Recently, we reported on the reaction characteristics of the ethanol oxidation reaction (EOR) over a carbon supported Pt/C fuel cell catalyst, which was studied under enforced and controlled electrolyte flow over a wide range of temperatures (23–100 °C) in a model study performed on a thin-film Pt/C catalyst electrode [21]. This study revealed drastic effects of the reaction temperature on the reaction characteristics. In particular, the selectivity for CO_2 formation was shown to increase to 45% (at 0.48 V, in 0.1 M acetaldehyde solution) for reaction at 100 °C, and temperatures of ~140 °C were estimated for reaching complete conversion to CO_2 [21]. For a further improved understanding of the reaction behavior in the DEFC, it would be highly desirable to also know the reaction behavior of the incomplete EOR products acetaldehyde and acetic acid under relevant, but nevertheless well-defined reaction and transport conditions at elevated temperatures. This is a topic of the present paper, where we report results of a high temperature/high pressure differential electrochemical mass spectrometry (HT/HP-DEMS) study in the same temperature range (23–100 °C).

Before going into details, we will briefly summarize the main findings on the adsorption and electrooxidation of acetaldehyde and acetic acid reported in previous studies [1,3,4,6,14,17,19,20,22–28]. Studying the acetaldehyde oxidation reaction (AOR) at a polycrystalline Pt electrode in acidic solution by *in situ* SNIFTIR spectroscopy, Rasch and Iwasita found that the main reaction products are CO_2 and acetic acid, with the product yield depending sensitively on the acetaldehyde

* Corresponding author. Tel.: +49 731 50 25451; fax: +49 731 50 25452.
E-mail address: juergen.behm@uni-ulm.de (R.J. Behm).
[1] Present address: Daimler AG, Germany.

0378-7753/$ – see front matter © 2012 Elsevier B.V. All rights reserved.
doi:10.1016/j.jpowsour.2011.12.024

concentration [23]. For the lowest acetaldehyde concentration (0.01 M), CO_2 was detected as the only reaction product, while for higher acetaldehyde concentrations (0.1 M and 1 M), both CO_2 and acetic acid were identified at comparable selectivities. The authors proposed that the pathway leading to CO_2 formation (in potential scans) is limited by the coverage of adsorbate species formed at low potentials. Rodríguez et al. [3] investigated the adsorption and oxidation of acetaldehyde on single-crystalline Pt(1 1 1) and Pt(1 0 0) electrodes by *in situ* FTIR spectroscopy, reporting CO_{ad} and adsorbed acetaldehyde/acetyl species formation. They suggested that CO_2 is produced via oxidation of strongly adsorbed intermediates, CO_{ad} and adsorbed acetaldehyde/acetyl species, but that none of these adsorbates is the intermediate in the pathway leading to acetic acid. Recently, Farias et al. [6] reported a systematic *in situ* FTIR spectroscopy study correlating the yields of CO_2 and acetic acid at polycrystalline Pt with the acetaldehyde concentration. They proposed that at high concentration (0.5 M), acetaldehyde molecules and water molecules compete for active sites, which increasingly hinders the oxidation of adsorbed species and thus the pathway to CO_2 formation. Adsorbed acetaldehyde/acetyl species were proposed to act as the decisive intermediate, which is responsible for the reaction branching to either dissociation at medium potentials (<0.5 V) or to oxidation to acetic acid (>0.7 V) [19]. These intermediate species were identified recently using surface enhanced FTIR spectroscopy in an attenuated total reflection (ATR) configuration [20,26,27]. Dissociative adsorption of acetaldehyde was confirmed to result in both CO_{ad} and CH_x species using *in situ* surface enhanced Raman spectroscopy [28] and ATR-FTIRS [20]. Adsorption and oxidation of acetaldehyde on carbon supported Pt/C catalysts [17,25] and on porous Pt and Rh electrodes [4,14] was also studied by DEMS. These studies revealed the formation of CO_{ad} and adsorbed hydrocarbon residues, where the latter species can be oxidized at potentials higher than 1.0 V or reductively desorbed as hydrocarbons upon hydrogen adsorption at low potentials. Based on the literature results, it is generally assumed that on Pt group metals acetaldehyde oxidation to CO_2 proceeds via oxidation of adsorbed species formed upon dissociative adsorption of acetaldehyde, with the total CO_2 product yield being in the range of a few percent at room temperature and at not too high potentials [17]. This was verified by a number of investigations on Pt/C [17,25] and PtRu/C or Pt_3Sn/C [17] catalyst electrodes, well-defined platinum single-crystal electrodes (Pt(1 1 1), Pt(1 0 0)) [3,19], on Pt thin film electrodes [20,26,28], and on Rh electrodes [4,14] (and references therein). At higher potentials, dissociative adsorption is increasingly hindered. At potentials >1.0 V it is essentially inhibited due to surface blocking by adsorbed oxy-species, which was concluded by comparison with previous FTIR results [6,20,26,28,29]. Under these conditions, oxidation of the formyl group to carboxyl leads to acetic acid formation.

Acetic acid adsorption/oxidation was also mainly studied at ambient temperatures on Pt electrodes [1,2,20,30]. Electrochemical, radiotracer and FTIR spectroscopy studies of the acetic acid adsorption behavior over polycrystalline and single crystalline platinum electrodes revealed a reversible adsorption of acetate anions in a twofold coordinated configuration, via the two oxygen atoms of the carboxyl group (see, e.g., [1,2,20,22,24,26]). The activity for C—C bond dissociation and further oxidation was found to be negligible at ambient temperatures. Therefore, formation of acetic acid was often assumed to be a "dead-end" in ethanol oxidation [31]. Thermally activated acetic acid oxidation on Pt was reported only at rather high temperatures, e.g., at 200 °C and above in an autoclave electrochemical cell [32].

Unfortunately, a direct transfer of these results to the reaction situation in a realistic fuel cell is hardly possible, since most of the model studies were performed at room temperature, while DEFCs are operated at elevated temperatures [7–12,33,34]. On the other hand, detailed studies of the reaction characteristics, in particular its selectivity, performed using realistic fuel cells, are rare [31,35]. Rao et al. [31] investigated ethanol oxidation, acetaldehyde oxidation and acetic acid oxidation in an operating fuel cell environment over Pt/C, PtRu/C and Pt_3Sn/C catalysts and showed that acetaldehyde is quite active for further oxidation, while acetic acid is resistant against further oxidation. Furthermore, a quantitative analysis of the product yields in a DEFC can be largely influenced by oxygen crossover from the cathode, resulting in additional oxidation of acetaldehyde to acetic acid, and/or losses of acetaldehyde due to crossover to the cathode side, both of which result in an apparent increase of the acetic acid yield at the anode [35]. In addition, the reaction conditions in a DEFC are generally much less defined than those in model studies, which may also lead to diverging results between different types of studies.

To bridge the gap between model studies and realistic fuel cell measurements, we recently developed a high-temperature/high-pressure DEMS set-up, which is based on an elevated temperature channel flow cell [36] interfaced to a mass spectrometer via a low-permeability Teflon membrane [37]. The set-up allows electrocatalytic measurements on supported catalyst thin-film electrodes (ca. 100% catalyst utilization, negligible diffusion limitations) at elevated temperatures (up to 100 °C) and pressure (3 bar overpressure) under continuous reaction and well-defined, enforced mass transport conditions. The complete oxidation product (CO_2) can be determined quantitatively, and it is thus possible to discriminate between partial and complete oxidation under realistic reaction conditions, which is particularly interesting for practical applications. Following previous studies of the electrooxidation behavior of small organic molecules such as ethanol [21], methanol [38], and ethylene glycol [39], this set-up was employed in the present work for a quantitative study of the activity/selectivity of the acetaldehyde oxidation reaction (AOR) and of the acetic acid oxidation reaction over a Pt/C catalyst at elevated temperatures and continuous reaction/mass transport conditions.

After a brief description of the experimental set-up and procedures (Section 2), we will present and discuss results of potentiodynamic (Section 3.1) and potentiostatic (Section 3.2) HT/HP-DEMS measurements in 0.1 M, 0.01 M and 0.001 M acetaldehyde solutions. The electrooxidation of acetic acid at constant potentials and elevated temperatures will be topic of Section 3.3. The apparent activation energies for the overall oxidation and for complete oxidation to CO_2 at different potentials, both for acetaldehyde and acetic acid, will be derived and discussed in Section 3.4. Finally, the mechanistic and kinetic implications arising from these data for realistic fuel cell operation will be discussed.

2. Experimental

2.1. High temperature DEMS setup and experimental details

The high temperature/high pressure DEMS set-up consisted of a differentially pumped two-chamber ultrahigh vacuum (UHV) system with a Balzers QMS 112 quadrupole mass spectrometer, a Pine Instruments potentiostat (model AFRDE5) and a computerized data acquisition system (for details see [37,40]). The electrochemical thin-layer channel flow cell and its mass transport characteristics were described recently [36]. The flow cell [36] was placed into an air thermostate and connected to a second thin-layer compartment, which interfaced the electrochemical cell to the UHV system containing the mass spectrometer via a thin, low-porosity Teflon membrane (10 μm thick). The electrolytes were supplied from pressurized glass bottles thermostated separately

in thermostats (Lauda E200), except for the acetaldehyde containing stock solution, which was maintained at room temperature. To minimize possible losses of acetaldehyde due to evaporation (b.p. 21 °C), the supporting electrolyte was first thoroughly deaerated by purging with N_2, and only then acetaldehyde was added to the desired concentration. Subsequently, the electrolyte was shortly purged again, pressurized with N_2 in the supply bottle, which was kept at room temperature, and then connected to an additional 50 mL glass reservoir, which was located in the air thermostat box directly before the flow cell and pre-filled with the same deaerated acetaldehyde solution. This way, we could maintain a constant concentration of acetaldehyde in the hot electrolyte during reaction, while otherwise the acetaldehyde concentration in the liquid decayed with increasing gas phase volume in the heated supply bottle due to evaporation into the gas phase. The electrolyte flow was controlled by a pressure-resistant syringe pump (Harward Apparatus 11plus).

A Pt wire served as counter electrode, an external saturated calomel electrode (SCE) kept at ambient temperature was used as reference electrode (for details see [36]). All potentials, however, were quoted against that of a reversible hydrogen electrode (RHE) for each respective reaction temperature [36,37].

The circular thin-film Pt/Vulcan (20 wt% metal, E-TEK Inc.) electrode was prepared following the procedure described in Ref. [41], by pipetting and drying 20 μL of an ultrasonically re-dispersed aqueous catalyst suspension (2 mg mL^{-1}) and then 20 μL of aqueous Nafion solution in the center of the mirror-polished planar glassy carbon rectangular plate (Sigradur G from Hochtemperatur Werkstoffe GmbH, 30 mm × 20 mm × 6 mm). This plate was mounted on the flow cell body and pressed against the gasket with the pre-cut channel (for details see [36]). The resulting catalyst thin film had a diameter of ca. 5 mm, an accessible geometric surface area of 0.2 cm^2, and a Pt loading of 40 μg_{Pt} cm^{-2}.

Prior to each measurement, the cell was carefully flushed with the supporting electrolyte, then the thin-film electrode was cycled in the potential range between 0.06 and 1.16 V (100 mV s^{-1} scan rate), until the cyclic voltammogram of a clean Pt/C electrode was reproduced [40]. The H_{upd} charge was used as an inherent reference to check for possible losses of catalyst after each experiment.

The supporting electrolyte was prepared using Millipore MilliQ water and suprapure sulfuric acid (Merck, suprapur). Acetaldehyde (≥99.5%, ACS reagent, Sigma–Aldrich), acetic acid (GR) and formic acid (GR for analysis) were obtained from Merck. Before the measurements, all solutions were deaerated by N_2. All experiments were carried out at an overpressure of 3 bar and at temperatures between 23 °C and 100 °C, as indicated.

2.2. Calibration and quantitative evaluation of the DEMS measurements

The use of a non-porous Teflon membrane, which inhibits the permeation of acetaldehyde, allows us to monitor the CO_2 partial pressure via the $m/z = 44$ signal without interference with the acetaldehyde signal at $m/z = 44$ [21].

The partial current for complete acetaldehyde electrooxidation to CO_2, $I_F(CO_2)$, was calculated using the following equation:

$$I_F(CO_2) = \frac{5 I_{MS}(m/z = 44)}{K^*_{44}} \quad (1)$$

where $I_{MS}(m/z = 44)$ is the mass spectrometric current of the $m/z = 44$ signal, the factor of 5 represents the average number of electrons needed for formation of one CO_2 molecule per C atom in acetaldehyde, and K^*_{44} is the calibration constant for $m/z = 44$, determined by potentiostatic HCOOH bulk oxidation at the respective temperatures. K^*_{44} was obtained via the relation:

$$K^*_{44} = \frac{2 I_{MS}(m/z = 44)}{I_F} \quad (2)$$

where I_F is the Faradaic current during HCOOH bulk oxidation and $I_{MS}(m/z = 44)$ is the mass spectrometric current, 2 is the number of electrons needed for formation of one CO_2 molecule from HCOOH. To remove effects from the temperature dependent permeability of the membrane, the CO_2 related $m/z = 44$ signals were normalized to the K^* value at room temperature, which were determined as reference before each series of measurements. The time delay between the onset in the production of gaseous species and their mass spectrometric detection (~4 s at a flow rate of 15 μL s^{-1}) was corrected for by using the difference in time response between onset of Faradaic current and the corresponding ion signal at $m/z = 44$ during the HCOOH oxidation at the respective temperature.

2.3. Experimental protocol

In the potentiodynamic experiments, the electrode potential was scanned in the range between 0.06 and 1.16 V at 10 mV s^{-1} scan rate. The potentiostatic measurements were performed as follows: after repetitive potential cycling, the potential was stopped at the low potential limit of 0.06 V during the negative-going scan and held for 5 min; then the potential was stepwise increased, first to 0.2 V, then in increments of 0.1 V to higher potentials with a waiting time of 5 min at each potential. Finally, the potential was stepped back to 0.06 V and held at this potential, until the ion signal at $m/z = 44$ reached a stable background level. The background drift was corrected based on the initial and final values at 0.06 V.

The current efficiency for CO_2 formation was calculated as the ratio of the partial current for acetaldehyde oxidation to CO_2 (see Eq. (1)), $I_F(CO_2)$, to the overall Faradaic current for acetaldehyde oxidation, using the quasi steady-state values at ~300 s. In the potentiodynamic measurements, the Faradaic currents shown in the corresponding figures were corrected for pseudo-capacitive contributions, which originated from double layer charging.

The apparent activation energies for acetaldehyde oxidation were calculated from the slopes in the Arrhenius plots of the partial currents for acetaldehyde oxidation to CO_2, $I_F(CO_2)$, and of the total Faradaic currents, respectively, at steady-state during potentiostatic acetaldehyde oxidation. Because of the very small rates for acetic acid oxidation, the Faradaic current and corresponding ion current at $m/z = 44$ were corrected for additional contributions, which may arise, e.g., from oxidation of the carbon support, by subtracting the respective currents measured in acetic acid free supporting electrolyte.

3. Results and discussion

3.1. Potentiodynamic oxidation of acetaldehyde

Fig. 1 shows potentiodynamic acetaldehyde oxidation traces recorded during continuous potential cycling (10 mV s^{-1} scan rate) in 0.5 M H_2SO_4 solution containing 0.1 M acetaldehyde at different temperatures (23, 40, 60, 80 and 100 °C). For more clarity, the cyclic voltammograms are presented as separate plots for the positive-going (Fig. 1a–c) and negative-going scans (Fig. 1d–f). Faradaic current traces (Fig. 1a and d), mass spectrometric ion current signals at $m/z = 44$ (Fig. 1b and e) and current efficiencies for CO_2 formation (Fig. 1c and f) are depicted in the upper, middle and bottom panels, respectively. The values of current efficiencies were calculated only for potentials, where the corresponding Faradaic current is above 1% of its maximum value. In the insets,

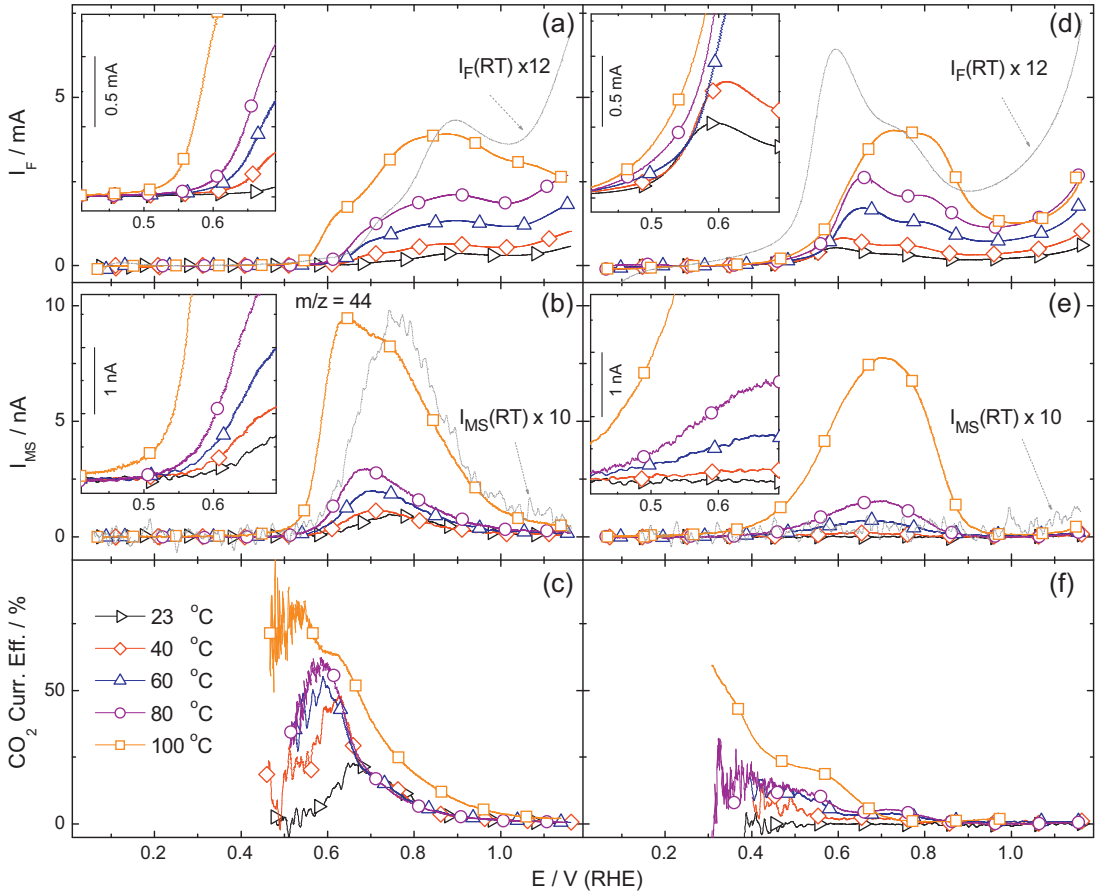

Fig. 1. Simultaneously recorded positive-going scan (a and b) and negative-going scan (d and e) of CVs (a and d) and MSCVs for $m/z = 44$ (b and d) and the corresponding CO_2 current efficiency (c and f) of the acetaldehyde oxidation reaction on a Pt/Vulcan catalyst in 0.1 M acetaldehyde solution pressurized with 3 bar N_2 overpressure at elevated temperatures (temperatures see figure). Dashed lines: magnified presentation of the room temperature traces (magnification factors see figure). Inset: magnified presentation of the reaction onset. Potential scan rate: 10 mV s^{-1}; catalyst loading: 40 μg_{Pt} cm^{-2}; electrolyte flow rate: 15 μl s^{-1}.

the Faradaic and mass spectrometric currents are shown at higher magnification. Furthermore, the room temperature CVs traces are shown for comparison on a magnified scale in the main panels.

At 23 °C, the general pattern of the Faradaic currents is similar to that reported previously under similar reaction and transport conditions over a Pt/C catalyst [17,25]. In the positive-going scan, the onset of acetaldehyde oxidation is largely suppressed at low potentials (<0.45 V, see inset), which is attributed to the presence of inhibiting adsorbed reaction intermediates, mainly CO_{ad} and $CH_{x,ad}$ species formed during the negative-going scan via dissociative adsorption of acetaldehyde [6,25,28]. At potentials above 0.45 V, the reaction starts and the Faradaic current increases, passes over a shoulder at ~0.73 V and reaches its maximum value at ~0.9 V (23 °C, see magnified current trace). The onset of the acetaldehyde oxidation corresponds to the onset of oxidation of acetaldehyde adsorbate (CO_{ad} at these potentials) [25]. After having passed the maximum, the acetaldehyde oxidation current decreases at higher potentials, which was attributed to an increasing hindrance for acetaldehyde dissociation, e.g., by adsorbed oxy-species formed at these potentials [3,17,20]. At potentials above 1.0 V, the acetaldehyde oxidation rate increases again, in contrast to the behavior of the EOR [21,26,42].

Increasing the temperature, we observed the following characteristic changes in the positive-going scan: (i) the Faradaic current increases significantly, by more than an order of magnitude from 23 °C (peak current 0.36 mA) to 100 °C (peak current 3.9 mA); (ii) the onset potential shifts negatively, from 0.45 V at 23 °C to ~0.42 V at 100 °C; (iii) the position of shoulder, centered at 0.73 V at 23 °C, also shifts negatively to about 0.6 V at 100 °C; (iv) the potential of the peak maximum shifts from ~0.9 V at 23 °C to 0.84 V at 100 °C. The thermal activation of the reaction, which agrees with similar tendencies in the temperature dependent ethanol oxidation reaction [21], can result from an activation of the C—C dissociation step, activation of the OH_{ad} formation, partial thermal desorption of the reaction inhibiting adsorbed intermediates [43], and/or activation of the reaction between the above reactants [44–51]. Comparing acetaldehyde oxidation with ethanol oxidation under identical reaction conditions [21], the peak current at 100 °C for acetaldehyde electrooxidation is ~4.5 times lower than that for ethanol electrooxidation under otherwise similar conditions. This is in agreement with the previous finding that the dissociative adsorption of acetaldehyde (C—C bond breaking) is more facile compared to ethanol adsorption, which was attributed to the higher polarity of the acetaldehyde molecule (aldehyde group vs. hydroxyl group) [25,28]. The resulting higher formation rate of adsorbed C1 species, which can irreversibly adsorb onto the electrode surface, results in a rapid poisoning of the surface at potentials where oxidation of these species is slow.

The corresponding Faradaic current patterns in the negative-going scans are shown in Fig. 1d. They differ distinctly from the positive-going scans in Fig. 1a. Starting from the anodic potential limit, the Faradaic currents first decrease, pass through a distinct minimum at ~0.9 V, then increase again after reduction of PtO, until reaching a current maximum at ~0.6 V via a shoulder located at ~0.75 V. Continuing the scan to more negative potentials, the Faradaic current decreases until it reaches the detection limit (at

100 °C at ~0.4 V, see inset in Fig. 1d). Upon increasing the temperature, the Faradaic current increases steadily, and at 100 °C the maximum current value is ~8 times higher than that at room temperature. The current profile develops with temperature from two resolved single peaks centered at 0.75 V and 0.6 V, respectively (both at 23 °C), to a broad single peak at 100 °C.

The CO_2 formation rate at $m/z = 44$ (Fig. 1b), after correction of the time delay between formation and detection (~4 s in our case, details see Section 2.2), first follows the Faradaic current traces. At 23 °C in the positive-going scan, the onset formation of CO_2 appears at around 0.5 V, followed by a steady increase of the ion current until reaching its maximum value at about 0.74 V. Then it decreases again to the background level, which is reached at 1.1 V. Hence, independent of the reaction temperature, CO_2 formation is inhibited at higher potentials. Accordingly, the increase of the Faradaic current at very positive potentials must be due to incomplete oxidation of acetaldehyde to acetic acid. These findings are in agreement with the spectroscopic detection of adsorbed acetate formation during acetaldehyde oxidation at potentials above 0.7 V, where the Pt surface is covered by significant amounts of OH_{ad} species [3,6,20,23,19,52]. Comparison with the Faradaic current peak reveals that the ion current peak coincides with the shoulder at ~0.73 V (at 23 °C) in the Faradaic current mentioned above (Fig. 1a). The low-potential shoulder was therefore ascribed to the complete oxidation of adsorbed species, which were formed at lower potentials, to CO_2 (mainly CO_{ad} oxidation at these potentials) [6,17,25,28,53]. With increasing reaction temperature, the onset potential of the CO_2 formation peak shifts negatively to 0.4 V at 100 °C, and the intensity in the ion current peak increases by one order of magnitude.

In the negative-going scan, CO_2 formation is completely suppressed over the entire potential range at ambient temperature (Fig. 1e). With increasing temperature (≥40 °C), CO_2 formation sets in and increases at potentials below 0.9 V. It reaches its maximum values at about 0.7 V, and then decreases again to the background level, which is reached at about 0.2 V. It should be noted that in contrast to the positive-going scan, the catalyst surface is initially oxidized in the negative-going scan when coming from higher potentials, and therefore the formation of CO_{ad} is hindered over a wide potential range [20,21,26]. In the positive-going scan, the temperature dependence of CO_2 formation reflects the temperature dependence of the oxidation of CO_{ad} pre-formed at lower potential, whereas in the negative-going scan, C—C bond rupture starts at potential where the resulting fragments can also be oxidized (negligible $C_{1,ad}$ coverage), and the temperature dependence reflects the combined temperature dependence of Pt surface reduction and C—C bond breaking.

The resulting patterns of the current efficiency for CO_2 formation are shown in Fig. 1c and f. In the positive-going scan (Fig. 1c), it exhibits a distinct temperature and potential dependence. Since acetaldehyde oxidation results only in two reaction products and one of them (CO_2) is detected quantitatively, the current efficiency for acetic acid formation can simply be deduced from the difference between 100% and the current efficiency for CO_2 formation. The CO_2 current efficiency exhibits its maximum at potentials between 0.5 and 0.7 V for all temperatures, followed by a subsequent decay at higher potentials. Increasing the temperature, the CO_2 current efficiency increases as well, reaching maximum values of ~80% at 100 °C (at ~0.57 V), while at 23 °C a maximum value of about 20% is reached at 0.66 V. As mentioned before, the Faradaic current at the onset of the current peak is largely attributed to the oxidation of acetaldehyde adsorbate, mainly CO_{ad}, which was formed at lower potentials and in the preceding negative-going scan. Since this results exclusively in CO_2 formation, it is not surprising that the maximum of the CO_2 current efficiency in the positive-going scan appears at the onset of the Faradaic current. Considering furthermore that the onset of pre-adsorbed CO_{ad} oxidation also shifts to lower potentials with increasing temperature [48,49,54], the earlier onset of the Faradaic current is easily explained. It also indicates that the down-shift of the onset potential with increasing temperature will allow oxidation to CO_2 via C—C bond breaking after the oxidation of CO_{ad} preformed at lower potentials, and also results in larger contribution to CO_2 formation than would be obtained in the absence of these preformed species. Hence, the earlier onset of the Faradaic current is partly or even largely an artifact of the potentiodynamic experiment, and would not be observed under potentiostatic reaction conditions (see Section 3.2). Similar observations were reported recently for ethanol oxidation under the same experimental conditions [21]. The decay of the CO_2 current efficiency at more positive potential indicates that at higher potentials the acetaldehyde oxidation reaction proceeds increasingly via an incomplete oxidation pathway (producing acetic acid). Finally, it is important to note that the apparent values obtained for the CO_2 current efficiency in the onset region of the Faradaic current in the positive-going scan are systematically too high: while the actual number of electrons required for oxidation of CO_{ad} pre-formed by dissociative adsorption of acetaldehyde at lower potentials is two, the calculations of the CO_2 current efficiency (Eq. (1)) assume five electrons per resulting CO_2 molecule when converting the mass spectrometric $m/z = 44$ current into the partial current for acetaldehyde oxidation to CO_2. Therefore, the actual values of the CO_2 current efficiency for acetaldehyde oxidation are lower than those shown in Fig. 1c.

In the negative-going scan (Fig. 1f), the current efficiencies for CO_2 formation increase steadily with decreasing potential, but remain at rather low levels. The maximum values range from ca. 10% at 60 °C to about 20% at 100 °C (both at 0.5 V). Since the electrode surface is initially free from reaction inhibiting adsorbed species during the negative-going scan after the reductive removal of OH_{ad}/oxide surface species, the increase of the CO_2 current efficiency between 0.6 and 0.45 V initially reflects the increasing activation for C—C bond breaking, until at lower potentials the build-up of strongly adsorbed species sets in. The apparent increase in the current efficiency for CO_2 formation at low potentials (below 0.4 V) in the negative-going scan results from an experimental artifact (for details see Ref. [21]).

In order to quantitatively determine the role of the acetaldehyde concentration on the activity and selectivity of the acetaldehyde oxidation reaction, we performed similar cyclic voltammetry DEMS measurements at lower acetaldehyde concentrations (0.01 and 0.001 M) under otherwise identical experimental conditions. The cyclic voltammograms for acetaldehyde oxidation in 0.01 M acetaldehyde solution (Fig. 2a–f) show an overall behavior rather similar to those obtained in 0.1 M solution, with an increased relative contribution of the lower potential peak in the Faradaic current in the positive-going scan, which becomes dominant at 0.01 M acetaldehyde concentration. For reaction in 0.001 M solution (Fig. 3a–f), the CVs exhibit distinct oxide reduction peaks in the potential range from 0.8 V to 0.9 V, overlapping with the acetaldehyde oxidation current in the negative-going scan. A quantitative evaluation of the electrooxidation behavior for different acetaldehyde concentrations at 100 °C shows:

(i) The maximum currents in the Faradaic current peaks decrease with decreasing concentration. In 0.01 M acetaldehyde solution, they are about 1/3 (positive-going scan) and 1/2 (negative-going scan) of those in 0.1 M solution, and in 0.001 M acetaldehyde solution, they are about 1/8 (positive-going scan) and 1/15 (negative-going scan).
(ii) The peak currents of the $m/z = 44$ ion signals also decrease with decreasing concentration, to about 1/2 (positive-going scan) and 2/5 (negative-going scan) of that in 0.1 M solution in 0.01 M

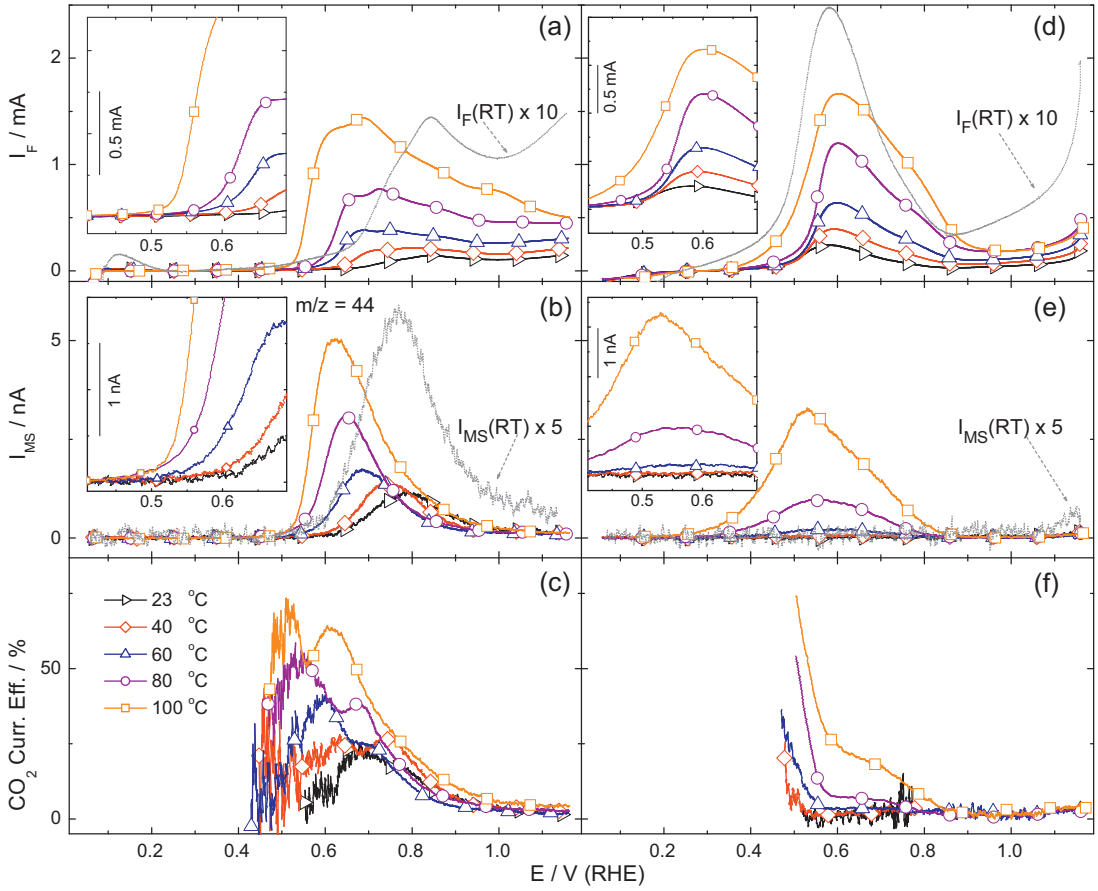

Fig. 2. Simultaneously recorded positive-going scan (a and b) and negative-going scan (d and e) of CVs (a and d) and MSCVs for $m/z = 44$ (b and d) and the corresponding CO_2 current efficiency (c and f) of the acetaldehyde oxidation reaction on a Pt/Vulcan catalyst in 0.01 M acetaldehyde solution. Dashed lines: magnified presentation of the room temperature traces (magnification factors see figure). Inset: magnified presentation of the reaction onset. Potential scan rate: 10 mV s^{-1}; catalyst loading: 40 μg_{Pt} cm^{-2}: electrolyte flow rate: 15 $\mu l\, s^{-1}$.

acetaldehyde solution, and to about 1/3 (positive-going scan) and 1/8 (negative-going scan) in 0.001 M acetaldehyde solution.

(iii) The onset potentials for acetaldehyde oxidation (both Faradaic current and $m/z = 44$ ion current signal) in the positive-going scan are shifted to lower potential with decreasing acetaldehyde concentration (see insets in the respective figures).

(iv) The peaks become narrower for lower concentrations, together with a distinct transition from broad two-state peaks to single-state peaks and the potential of the peak maximum also shifts negatively. On the other hand, the tendency of the CO_2 current efficiency change with potential is similar for all concentrations. The maximum values of the CO_2 current efficiencies, however, are different. Taking the results at 100 °C for example, they are 68% (at 0.53 V) in 0.01 M acetaldehyde solution, while in 0.001 M acetaldehyde solution, they are 85% (at 0.49 V), respectively (all values for the positive-going scan).

Hence, for all concentrations the current efficiencies for CO_2 formation at 100 °C and at 0.6 V in the positive-going scan are in the range between 50% and 60%. At higher potentials, the oxidation of acetaldehyde on the OH_{ad}/oxide covered surface produces large amounts of incomplete oxidation species (acetic acid) in 0.1 and 0.01 M acetaldehyde solution. For very low acetaldehyde concentrations (1 mM), however, the reaction rate becomes significantly lower, which in turn leads to a visible oxide reduction peak in the subsequent negative-going scan (Fig. 3d).

The potential-dependent variation of the current efficiency for CO_2 formation in the acetaldehyde oxidation confirms that both the overall and partial reaction rates are controlled by the potential-dependent composition and coverage of the adlayer and by potential effects on the kinetically limited surface processes. At lower potentials (<0.5 V), the coverage of adsorbed C_1 species resulting from dissociative acetaldehyde decomposition is higher and inhibits the onset of acetaldehyde oxidation; at medium potentials ($0.5\,V \le E \le 0.7\,V$), the coverage of CO_{ad} decreases due to CO_{ad} oxidation, and at even more positive potentials ($E > 0.7$ V), the coverage of CO_{ad} decreases further, due to more efficient CO_{ad} oxidation and decreasing CO_{ad} formation (C—C bond dissociation) on the oxy-species covered surface. The latter results in the change of the selectivity towards acetic acid formation, in agreement with the observation of adsorbed acetate species during acetaldehyde oxidation at high potentials by FTIRS [3,20] or SERS [28] measurements.

3.2. Potentiostatic oxidation of acetaldehyde

In order to deconvolute kinetic (reaction rate) and dynamic (linear variation of the electrode potential) effects, which both contribute to the potentiodynamic measurements, and to avoid effects caused by different coverages of the adsorbed species depending on the potential scan direction, we performed a series of potentiostatic experiments, monitoring simultaneously both the Faradaic current (Fig. 4a) and the mass spectrometric ion current for CO_2 formation ($m/z = 44$, Fig. 4b) at different constant electrode potentials

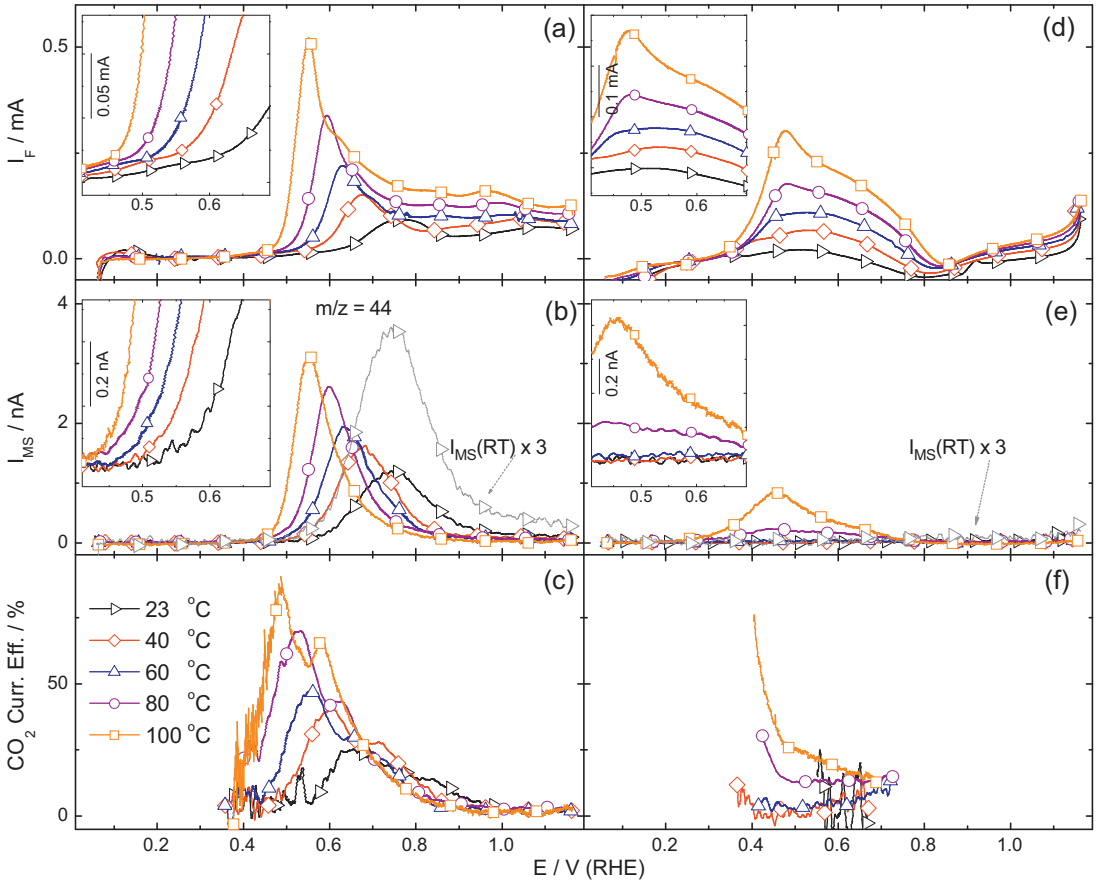

Fig. 3. Simultaneously recorded positive-going scan (a and b) and negative-going scan (d and e) of CVs (a and d) and MSCVs for $m/z = 44$ (b and d) and the corresponding CO_2 current efficiency (c and f) of the acetaldehyde oxidation reaction in 0.001 M acetaldehyde solution. Dashed lines: magnified presentation of the room temperature traces (magnification factors see figure). Inset: magnified presentation of the reaction onset. Potential scan rate: 10 mV s^{-1}; catalyst loading: 40 μg_{Pt} cm^{-2}; electrolyte flow rate: 15 $\mu l\, s^{-1}$.

and different reaction temperatures in 0.1 M acetaldehyde solution. The resulting current efficiencies for CO_2 formation are plotted in Fig. 4c (for details see Section 2.2).

For all temperatures, both Faradaic current (Fig. 4a) and the mass spectrometric current for CO_2 formation ($m/z = 44$, Fig. 4b) are below the detection limit at potentials below 0.4 V. This agrees fully with the results obtained in the potentiodynamic measurements (see Section 3.1).

Small Faradaic currents as well as mass spectrometric CO_2 signals were detected at 0.5 V at higher temperatures (≥80 °C, see insets in Fig. 4a and b), reflecting the thermal activation of the reaction under these conditions. (The current efficiencies for CO_2 formation below 80 °C at 0.5 V are not shown in the figures because of the poor signal-to-noise ratio.) At 0.6 V, the Faradaic current for acetaldehyde oxidation increases steeply after the potential step, followed by a corresponding increase in the mass spectrometric current for CO_2 formation. At 0.7 V, the Faradaic current first increases and then decreases steadily until approaching a stable value after about 300 s. The corresponding mass spectrometric CO_2 signals closely follow the Faradaic current transients. The initial maximum in the CO_2 ion current signal is attributed to the fast oxidation of the CO_{ad} which was produced at lower potential, before the potential step. Similar series of potentiostatic measurements were performed also in 0.01 M (Fig. 5) and in 0.001 M (Fig. 6) acetaldehyde solution to evaluate the effect of acetaldehyde concentration on the activity and selectivity of the acetaldehyde oxidation reaction.

The general profiles of the current transients for constant potential oxidation for the dilute solutions are rather similar to those in 0.1 M acetaldehyde solution discussed above. While the steady-state Faradaic current increases by factors of 6.7 and 4.7 when going from 0.5 to 0.6 V and from 0.6 to 0.7 V, respectively, in 0.1 M acetaldehyde solutions, the respective values are 5.6/1.5 and 1/0.7 in 0.01 M and 1 mM acetaldehyde solution (all at 100 °C). A similar comparison of the corresponding CO_2 ion signals results in a comparable trend for 0.1 M acetaldehyde solution, while for 0.01 M acetaldehyde solution, the signal decreases when going from 0.6 to 0.7 V. Finally, for 0.001 M acetaldehyde solution, this signal decreases already when going from 0.5 to 0.6 V, opposite to the tendency in the Faradaic current, and going to 0.7 V, also the CO_2 formation ion current continues to decrease, following the behavior of the Faradaic current, but more pronounced. We attribute these distinct differences in the behavior of the Faradaic current and the corresponding CO_2 ion current with acetaldehyde concentration and potential to differences in the composition and coverages of the adlayer, which in turn will affect the activity and selectivity of the reaction.

The corresponding current efficiencies for CO_2 formation, calculated from the steady-state currents at about 300 s, are listed in Table 1. For 0.1 M acetaldehyde solution, this increases up to ~80% at 100 °C and 0.5 V. At 0.6 V, the CO_2 current efficiencies are generally lower than at 0.5 V, increasing from 7% at r.t. to 39% at 100 °C, while the absolute currents are much higher. The increase of the CO_2 current efficiency with increasing temperature and decreasing potential (see Table 1) resembles previous findings for the oxidation

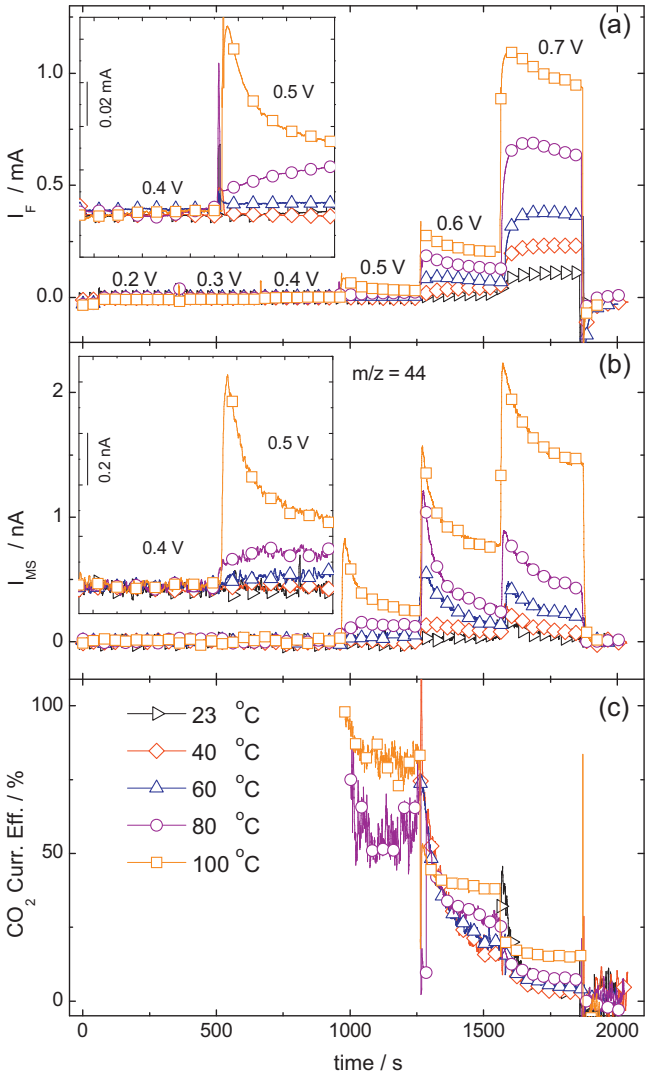

Fig. 4. Simultaneously recorded transients of the Faradaic current (a) and the CO_2 ion currents for $m/z = 44$ (b), and the corresponding current efficiency for CO_2 formation (c) during potentiostatic oxidation of acetaldehyde on a Pt/Vulcan catalyst in 0.1 M acetaldehyde solution at elevated temperatures (temperatures see figure). Catalyst loading: 40 μg_{Pt} cm^{-2}; electrolyte flow rate: 15 $\mu l\, s^{-1}$.

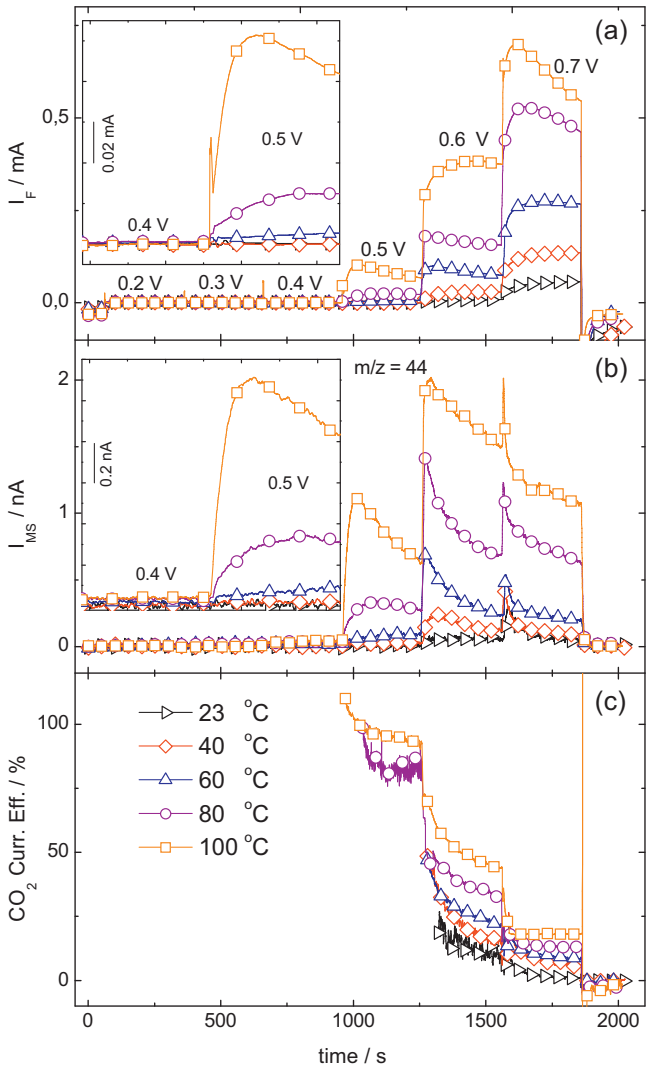

Fig. 5. Simultaneously recorded transients of the Faradaic current (a) and the CO_2 ion currents for $m/z = 44$ (b), and the corresponding current efficiency for CO_2 formation (c) during potentiostatic oxidation of acetaldehyde on a Pt/Vulcan catalyst in 0.01 M acetaldehyde solution. Catalyst loading: 40 μg_{Pt} cm^{-2}; electrolyte flow rate: 15 $\mu l\, s^{-1}$.

of ethanol or ethylene glycol on a Pt/C catalyst [21,39]. The temperature dependence and its implications will be discussed in detail in Section 3.4.

Comparing the steady-state current efficiencies for CO_2 formation at constant potentials with the results obtained in potentiodynamic measurements at the same potential shows significant discrepancies. For reaction in 0.1 M acetaldehyde solution at 100 °C and 0.6 V, the corresponding current efficiency is about 40% in potentiostatic measurements vs. ~60% in potentiodynamic measurements. The difference between these two measurements simply reflects the differences in the adlayer composition and coverage and their effect on the selectivity of the reaction.

For 0.01 M acetaldehyde solution, the resulting current efficiencies for CO_2 formation are comparable to those in 0.1 M solution, yielding values between ca. 10% at 23 °C and ~40% at 100 °C at 0.6 V (7% and 39% in 0.1 M solution). Interestingly, the CO_2 current efficiencies decrease when going to 0.001 M acetaldehyde solutions, where we obtain values between 6% (23 °C) and 30% (100 °C) at 0.6 V (see Table 1).

Distinct concentration effects on the CO_2 current efficiency were observed also for ethanol oxidation on similar Pt/C catalyst electrodes, and at least partly attributed to transport effects, to the higher chance of re-adsorption and further reaction of the incomplete reaction product (acetaldehyde) to CO_2 in more dilute solutions [21] ('desorption–re-adsorption–further reaction' concept, see Refs. [55–57]). For the present case, contributions from re-adsorption of incomplete oxidation products can be excluded, since the only incomplete oxidation product, acetic acid, does not react further at present reaction conditions (see next section). In this case, the variation of the current efficiency upon changes in the acetaldehyde concentration can only be due to differences in the composition and (partial) coverage of the adlayer in different reaction solutions, which directly affects the selectivity for C—C bond breaking vs. oxidation of the functional —CHO group. The influence of the adlayer on the selectivity is reflected also by the significant difference in CO_2 current efficiencies and hence in selectivity obtained in potentiostatic and potentiodynamic measurements. In the latter case, the convolution of potential and time effects results in a different adlayer composition than obtained under steady-state conditions at constant potential. Similar effects are also responsible for the variation of the CO_2 current efficiency with time during

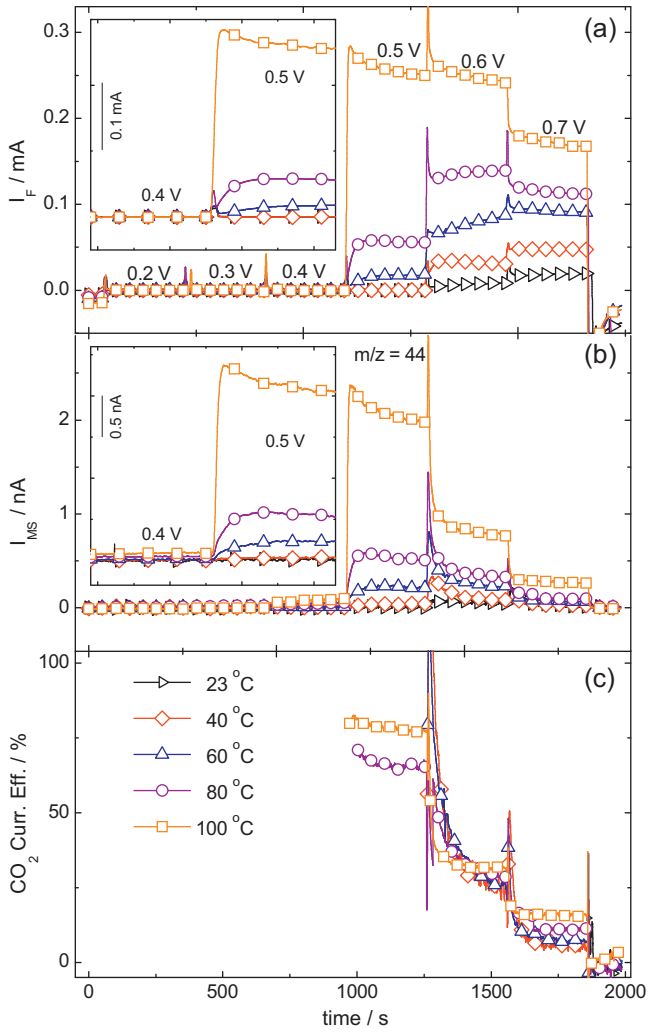

Fig. 6. Simultaneously recorded transients of the Faradaic current (a) and the CO_2 ion currents for $m/z = 44$ (b), and the corresponding current efficiency for CO_2 formation (c) during potentiostatic oxidation of acetaldehyde on a Pt/Vulcan catalyst in 0.001 M acetaldehyde solution. Catalyst loading: 40 μg_{Pt} cm^{-2}; electrolyte flow rate: 15 $\mu l\, s^{-1}$.

the reaction transients, which are particularly pronounced at low potential (0.5 V).

Increasing the potential to 0.7 V results in a significant decrease of the CO_2 current efficiencies for all concentrations and temperatures, without modifying the general trends for the temperature and concentration dependence discussed above. As will be discussed in more detail, in Section 3.4, we associate this with a gradual change in the rate limiting step, from CO_{ad} oxidation at lower potentials to C—C bond breaking at higher potentials. This in turn results in distinct changes in the adlayer composition, in particular in the coverage of reaction inhibiting CO_{ad} species.

Table 1
Steady-state current efficiencies for CO_2 formation (in percent) during potentiostatic acetaldehyde oxidation at different concentrations, potentials and temperatures.

T/°C	0.1 M acetaldehyde		0.01 M acetaldehyde		0.001 M acetaldehyde	
	0.6 V	0.7 V	0.6 V	0.7 V	0.6 V	0.7 V
23	7 ± 0.2	4 ± 0.1	9 ± 0.4	5 ± 0.2	6 ± 0.3	4 ± 0.2
40	11 ± 0.6	5 ± 0.3	15 ± 0.7	6 ± 0.2	16 ± 0.6	5 ± 0.3
60	20 ± 1	7 ± 0.3	21 ± 1	9 ± 0.4	23 ± 0.8	8 ± 0.6
80	27 ± 1	9 ± 0.5	29 ± 2	12 ± 1	26 ± 1	11 ± 0.6
100	39 ± 2	15 ± 0.8	41 ± 3	17 ± 1	31 ± 2	16 ± 1

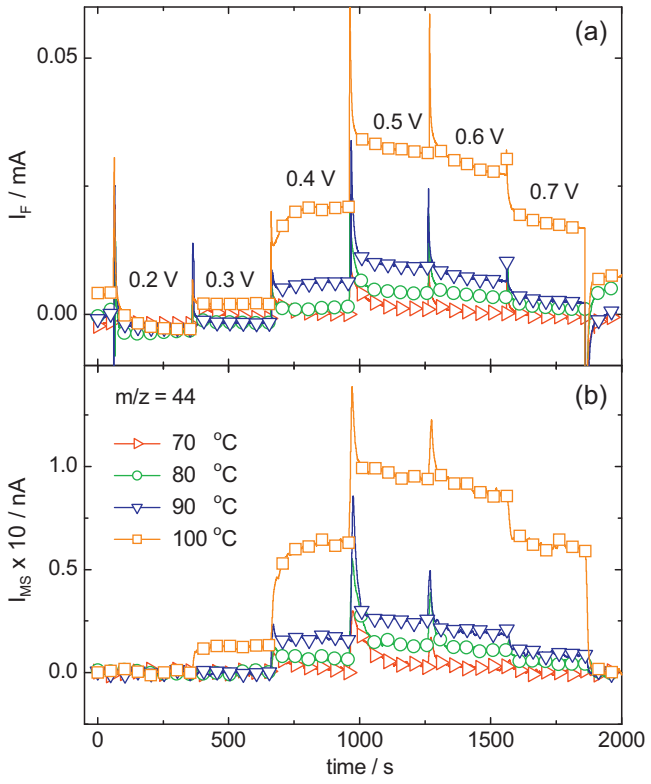

Fig. 7. Simultaneously recorded transients of the Faradaic current (a) and the CO_2 ion currents for $m/z = 44$ (b) during potentiostatic oxidation of acetic acid on a Pt/Vulcan catalyst in 0.1 M acetic acid solution at elevated temperatures (temperatures see figure). Catalyst loading: 40 μg_{Pt} cm^{-2}; electrolyte flow rate: 15 $\mu l\, s^{-1}$.

In total, the potentiostatic measurements revealed comparable trends in the reactivity and CO_2 selectivity as obtained in the potentiodynamic measurements; on a quantitative scale, however, the data differ significantly. This is attributed to the significant differences in the adlayer coverages and compositions in the two cases. Since the steady-state values obtained under potentiostatic conditions are free from dynamic variations in the adlayer, they are much better suited for comparison with fuel cell measurements.

3.3. Potentiostatic oxidation of acetic acid

In order to quantitatively determine the CO_2 formation in acetic acid oxidation under steady-state reaction conditions, a series of potentiostatic experiments was performed, monitoring the Faradaic current (Fig. 7a) and the mass spectrometric ion current for CO_2 formation (at $m/z = 44$, Fig. 7b) at different electrode potentials (from 0.2 V to 0.7 V) and different reaction temperatures. Because of the very low oxidation rates, measurements were performed only at temperatures ≥70 °C and for 0.1 M acetic acid concentration and the corresponding data were corrected (for details see Section 2).

At temperatures below 90 °C, both the Faradaic current (Fig. 7a) and the mass spectrometric ion current for CO_2 formation ($m/z = 44$, Fig. 7b) are extremely low compared with the current in acetaldehyde oxidation, which shows that acetic acid is very stable towards C—C bond splitting and oxidation to CO_2 under these conditions. These results agree with previous findings for acetic acid (1 M acetic acid solution) oxidation at different temperatures (101 °C, 152 °C, 195 °C and 249 °C) on a Pt electrode, where measurable rates were observed only at temperatures above 200 °C [32]. At 100 °C, the Faradaic current and ion signal increased significantly, though their absolute values are still much lower than those for acetaldehyde

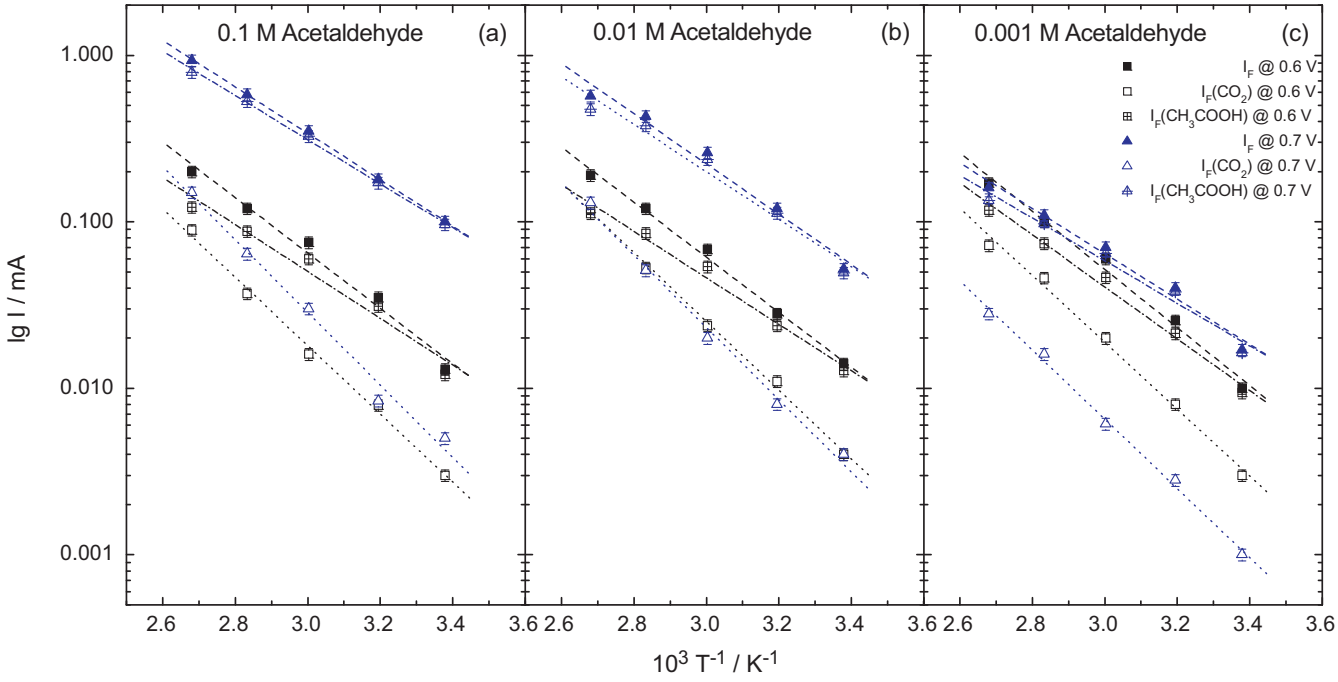

Fig. 8. Arrhenius plots of the overall acetaldehyde oxidation rate (Faradaic current) of the complete oxidation of acetaldehyde to CO_2 (partial current for CO_2 formation) and of the incomplete oxidation to acetic acid (with assumption the products for acetaldehyde oxidation are only CO_2 and acetic acid) in 0.1 M acetaldehyde solution (a), 0.01 M acetaldehyde solution (b) and 0.001 M acetaldehyde solution (c) at different potentials (potentials see figure). The precision in the current measurements is approximately ±15% in the Faradaic currents and ±9% in the mass spectrometric CO_2 signals. Electrolyte flow rate: 15 μl s^{-1}; catalyst loading: 40 μg_{Pt} cm^{-2}.

Table 2
Apparent activation energies for the overall acetaldehyde oxidation reaction (Faradaic current), complete oxidation to CO_2 (CO_2 partial reaction current) and incomplete oxidation to acetic acid (derived by assuming that CO_2 and acetic acid are the only products for acetaldehyde oxidation) at different acetaldehyde concentrations and potentials, determined from the steady-state reaction currents.

E/V	0.1 M acetaldehyde			0.01 M acetaldehyde			0.001 M acetaldehyde		
	E_a/kJ mol^{-1}	$E_a(CO_2)$/kJ mol^{-1}	$E_a(CH_3COOH)$/kJ mol^{-1}	E_a/kJ mol^{-1}	$E_a(CO_2)$/kJ mol^{-1}	$E_a(CH_3COOH)$/kJ mol^{-1}	E_a/kJ mol^{-1}	$E_a(CO_2)$/kJ mol^{-1}	$E_a(CH_3COOH)$/kJ mol^{-1}
0.6	32 ± 2	39 ± 2	27 ± 3	34 ± 2	40 ± 2	27 ± 2	33 ± 1	38 ± 1	29 ± 2
0.7	27 ± 1	42 ± 1	25 ± 1	29 ± 3	42 ± 2	26 ± 3	26 ± 1	40 ± 1	25 ± 2

oxidation (Fig. 4) or ethanol oxidation [21]. Thus, contributions from acetic acid oxidation can be neglected in those reactions under present reaction conditions, i.e., oxidation of acetic acid formed by incomplete oxidation of ethanol or acetaldehyde can be neglected under present reaction conditions, at temperatures up to 100 °C and on supported Pt catalysts. This agrees with the general perception that formation of acetic acid is a dead end in ethanol oxidation [19,20,31,58].

3.4. Apparent activation energies

The apparent activation energies for the overall acetaldehyde oxidation reaction and for the complete oxidation of acetaldehyde to CO_2, E_a and $E_a(CO_2)$, respectively, which were derived from the Arrhenius plots of the steady-state Faradaic currents and of the steady-state mass spectrometric ion currents at $m/z = 44$ for different acetaldehyde concentrations and at the respective reaction potentials (Fig. 8), are listed in Table 2 (for details see Section 2.2). Furthermore, we also calculated the apparent activation energy for the incomplete oxidation of acetaldehyde to acetic acid from the Arrhenius plots for the partial oxidation currents for acetic acid formation. The latter were calculated from the difference between the total reaction current and the partial reaction current of the complete oxidation to CO_2 (Fig. 9).

The linear decay of the logarithmic oxidation rates with $1/T$ implies that the rate determining step does not change with temperature. One has to keep in mind, however, that the overall reaction contains contributions from C—C bond splitting and CO_2 formation as well as from incomplete acetaldehyde oxidation to

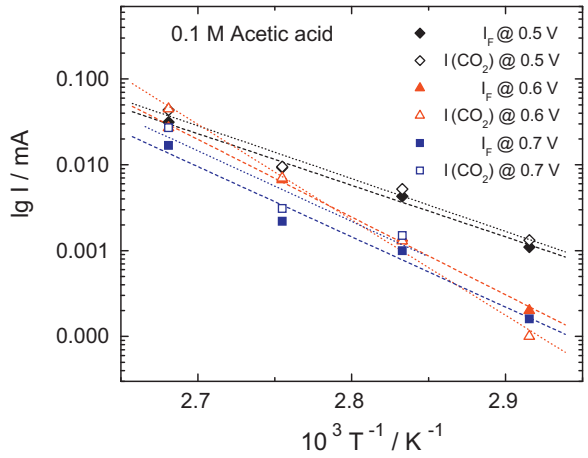

Fig. 9. Arrhenius plots of the overall acetic acid oxidation rate (I_F) and of the complete oxidation of acetic acid to CO_2 ($I_F(CO_2)$) in 0.1 M acetic acid solution at different potentials (potentials see figure). The mass spectrometric CO_2 signals at 70 °C and 0.6 as well as at 0.7 V are too low to be reliably evaluated and therefore not shown. Electrolyte flow rate: 15 μl s^{-1}; catalyst loading: 40 μg_{Pt} cm^{-2}.

Table 3
Apparent activation energies for the overall acetic acid oxidation (0.1 M) reaction (Faradaic current) and complete oxidation to CO_2 (CO_2 partial reaction current) at different potentials, determined from steady-state reaction currents.

E/V	0.1 M acetic acid	
	E_a/kJ mol^{-1}	$E_a(CO_2)$/kJ mol^{-1}
0.5	115 ± 8	118 ± 13
0.6	173 ± 6	196 ± 7
0.7	157 ± 18	158 ± 48

acetic acid, and even the incomplete reaction to acetic acid contains more than one reaction step. Therefore, these other reaction steps and also effects of the adlayer coverage and composition have to be considered in the complete reaction kinetics. This is most obvious for the overall oxidation of acetaldehyde. Here we know that the CO_2 current efficiency increases with increasing temperature and therefore the contributions of the two pathways change with temperature. Therefore, the measured barrier cannot be associated with a single reaction step, but is an apparent barrier value reflecting the overall temperature dependence of the reaction network (Table 3).

The close similarity between the values of the apparent activation barrier for incomplete oxidation to acetic acid at different acetaldehyde concentrations (27 ± 3 kJ mol^{-1} at 0.6 V and 26 ± 3 kJ mol^{-1} at 0.7 V) and for complete oxidation to CO_2 (39 ± 3 kJ mol^{-1} at 0.6 and 42 ± 3 kJ mol^{-1} at 0.7 V) indicates that the temperature dependence of the rate limiting step in these reaction pathways is largely independent of the acetaldehyde concentration. For the overall reaction, the close similarity of the values of E_a (33 ± 3 kJ mol^{-1} at 0.6 V and 29 ± 3 kJ mol^{-1} at 0.7 V) for different acetaldehyde concentrations seem to indicate a similar situation; in this case, however, it reflects the temperature dependence of the entire reaction network with its two reaction pathways (see above Section 3). In a more detailed discussion, one has to add that also the temperature dependence of the incomplete oxidation reaction to acetic acid may be dominated by the removal of CO_{ad}, via the steady-state coverage of CO_{ad}, and hence by OH_{ad} formation and reaction with CO_{ad}. This step can be dominant if the reaction is limited by the number of vacant sites available for acetaldehyde adsorption and subsequent dissociation. Finally, it should be noted that the effective activation energy for catalytic gas phase oxidation of acetaldehyde, using O_2 as oxidant, is significantly higher than the value determined here for acetaldehyde oxidation, with about 55 kJ mol^{-1} [59] vs. about 40 kJ mol^{-1} in the present work.

The potential dependence of the apparent activation energies is characterized by a subtle decrease of the values for $E_a(CH_3COOH)$ and a similar size increase of $E_a(CO_2)$ when going from 0.6 V to 0.7 V reaction potential. In total, this results in a comparable size decrease of the apparent activation barrier E_a for the overall reaction at both potentials (see Table 2). The combination of a decreasing apparent activation energy for acetic acid formation and an increasing apparent activation energy for CO_2 formation at higher potential leads to a change in the selectivity of the reaction towards predominant acetic acid formation at higher potential, which is reflected by the decrease in current efficiency for CO_2 formation with increasing potential. We assume that these changes result at least partly from a gradual transition in the rate limiting step with potential. At lower potentials, oxidative removal of CO_{ad}, which is strongly influenced by the potential dependent OH_{ad} formation, is rate limiting, while at higher potential CO_{ad} oxidation is increasingly faster and C—C bond rupture becomes rate limiting. If the latter process is associated with a higher reaction barrier than OH_{ad} formation/CO_{ad} oxidation, this change in the rate limiting step results in the observed increase of the apparent activation energy for CO_2 with increasing potential. Furthermore, with increase in potential and temperatures, adsorption of oxy-species and sulfates reduces the number of larger adsorbate-free Pt ensembles required for the dissociative adsorption of acetaldehyde to form CO_{ad}, while smaller ensembles sufficient for oxidizing the functional group to carboxyl are still available [60].

The still rather low values of $E_a(CO_2)$ obtained at 0.7 V, which were tentatively associated with C—C bond rupture, indicate that even for this reaction step the barrier is much smaller than the C—C bond energy (354.8 ± 1.7 kJ mol^{-1} in acetaldehyde [61]), i.e., C—C bond breaking in adsorbed acetyl [20] proceeds in a highly correlated process, where simultaneous bond formation between the resulting fragments and the Pt nanoparticles leads to a pronounced reduction of the barrier compared to the C—C bond energy. The barrier for C—C bond rupture in acetaldehyde is significantly lower than the barrier for complete oxidation of ethanol to CO_2 at ~0.7 V under similar conditions (65 ± 3 kJ mol^{-1} in 0.1 M ethanol solution) [21]. Apparently, in the latter case, simultaneous bond formation of the fragments with the Pt particles is less efficient than for adsorbed acetaldehyde, resulting in a higher barrier of the C—C bond rupture step. Investigating the mechanism of ethanol oxidation, especially the selectivity of this reaction, on different Pt surfaces with density functional theory based calculations, Wang and Liu calculated reaction barriers for C—C bond breaking of ethanol is 287.5 kJ mol^{-1}, while C—C for adsorbed acetyl this value is much lower (131.2 kJ mol^{-1}) [62]. They also found that CO_2 and acetic acid originate from the same surface intermediate, CH_3CO_{ad}, in agreement with previous experimental findings [20], and that C—C bond breaking occurs predominantly via strongly adsorbed CH_2CO or CHCO intermediates on defect sites rather than directly from CH_3CO_{ad} on the flat Pt(1 1 1) terraces. The CH_2CO_{ad} or $CHCO_{ad}$ intermediates were formed before by CH_3CO dehydrogenation.

The apparent activation energies for acetic acid oxidation, as measured by the Faradaic current and by the CO_2 mass spectrometric signal are in the range of ~115–180 kJ mol^{-1}. (Note that the mass spectrometric currents at 70 °C and 0.6/0.7 V were too low to be reliably evaluated and therefore not used for the determination of the activation barrier.) As expected from the fact that CO_2 is the only reaction product, the values for the activation energy determined from the Faraday current and from the mass spectrometric CO_2 signal agree reasonably well. The very high values indicate that in this case the simultaneous bond formation, together with C—C bond breaking is much less efficient than for Pt catalyzed C—C bond breaking in other molecules such as ethanol [21] or acetaldehyde (see above). To overcome the reaction barrier for acetic acid oxidation on a Pt electrode, much higher temperatures (above 200 °C) are required according to the literature data [32].

The above data confirm the existing picture that formation of acetic acid during acetaldehyde oxidation, and similarly also for ethanol oxidation, is a 'dead-end', where further oxidation is not possible under common reaction conditions [19,20,28,58]. C—C bond breaking has to occur in the preceding reaction steps, e.g., during interaction of the surface with adsorbed acetyl species [20]. Once acetic acid is formed, it is essentially stable even at 100 °C.

3.5. Implications for direct ethanol fuel cell operation

The results reported in the previous sections have considerable implications on the understanding and optimization of DEFCs. Assuming that ethanol oxidation proceeds at least partly via formation of adsorbed acetaldehyde/acetyl species, which can subsequently desorb (acetaldehyde formation) or continue reaction to acetic acid or CO_2, the oxidation of acetaldehyde is a crucial step in the reaction sequence.

First, it is important to note that increasing reaction temperatures not only result in a higher reaction rate, but, due to the higher activation barrier for complete oxidation of acetaldehyde to CO_2

compared to its partial oxidation, also in a decreasing amount of acetic acid formation. Extrapolating the data in Fig. 8 to higher temperatures, one can estimate that under current reaction conditions and at 0.6 V, complete conversion to CO_2 will be reached at about 364 °C (0.1 M solution), provided there is no change in the reaction mechanism and rate determining pathways. For higher potentials, this temperature will shift to lower values (~340 °C at 0.7 V). It is interesting to note that while acetaldehyde adsorption (CO_{ad} formation) on Pt is much more facile at ambient temperature and also less potential dependent that ethanol oxidation, the increase of the CO_2 current efficiency is much steeper for ethanol oxidation, resulting in a much lower temperature for complete conversion to CO_2 of ~175 °C at 0.6 V (140 °C at 0.5 V) [21].

Acetic acid formation has to be avoided at the stage of acetaldehyde/acetyl interaction with the active Pt nanoparticles, since once formed its later oxidation is essentially impossible under realistic fuel cell reaction conditions. Since ethanol oxidation is likely to proceed via adsorbed acetyl/acetaldehyde formation, the selectivity of acetaldehyde oxidation to CO_2 is a prime objective in the optimization of anode catalysts for DEFCs.

Second, considering possible improvements in the anode catalyst, one has to keep in mind that this has to activate not only C—C bond breaking, but also the oxidative removal of the resulting adsorbed fragments CO_{ad} and $CH_{x,ad}$ to CO_2. Only if the removal of these species is not rate limiting, a further increase of the C—C bond breaking rate will lead to an overall improvement of the reaction kinetics, i.e., a higher oxidation current. Otherwise, the increasing steady-state coverage of CO_{ad} and $CH_{x,ad}$ species will result in an effective decrease of the oxidation current. In that sense, catalysts with an improved activity for C—C bond breaking are not beneficial for the acetaldehyde oxidation reaction, unless they are also more active for oxidation of adsorbed CO_{ad} and $CH_{x,ad}$ species. These conclusions are equally correct also for ethanol oxidation. In that sense, bimetallic catalysts with improved CO_{ad} oxidation properties compared to Pt/C such as PtSn/C or PtRu/C [7,12,17,31] are beneficial for complete oxidation of ethanol or acetaldehyde to CO_2 only if they are also more active for C—C bond breaking. So far, this latter question is still open for reaction at elevated temperatures. Recently, Kowal et al. presented a Pt/Rh/SnO_2 catalyst, which according to their claims was more active in both partial reaction steps in ethanol oxidation and which may be a promising step forward [63,64].

4. Conclusions

Potentiodynamic and potentiostatic DEMS measurements of the acetaldehyde and acetic acid oxidation reactions on carbon supported Pt/Vulcan thin-film catalyst electrodes performed under fuel cell relevant, but nevertheless well-defined reaction and transport conditions (controlled electrolyte transport, continuous reaction, elevated temperatures and pressure) and on relevant materials (supported catalysts, 100% catalyst utilization), led to the following conclusions:

1. For acetaldehyde oxidation, both the overall reaction rate, as measured by the Faradaic current, and the rate for CO_2 formation increase significantly with increasing reaction temperature. The increase with temperature is more pronounced for complete oxidation to CO_2 than for the overall acetaldehyde oxidation reaction. Correspondingly, the apparent activation energies are higher for CO_2 formation than for the overall reaction (39 ± 2 kJ mol^{-1} vs. 32 ± 2 kJ mol^{-1} in 0.1 M acetaldehyde solution, 0.6 V).
2. In the same way, also the current efficiency for CO_2 formation under steady-state conditions (during acetaldehyde oxidation) increases significantly with temperature, in particular at temperatures >60 °C, from negligible CO_2 formation (7%) at room temperature to 39% at 100 °C (0.6 V). Accordingly, the formation of the incomplete oxidation product acetic acid, which is dominant at ambient temperature, decreases significantly with temperature. High values of the current efficiency for CO_2 formation over the Pt/C catalyst can be reached, however, only at low potentials (0.5 V) and hence at rather low current densities (geometric surface area normalized current density): 81 ± 3% at 0.16 mA cm^{-2} (0.5 V, 0.1 M acetaldehyde solution), 93 ± 4% at 0.34 mA cm^{-2} (0.5 V, 0.01 M acetaldehyde solution), and 77 ± 3% at 1.25 mA cm^{-2} (0.5 V, 0.001 M acetaldehyde solution) (all at 100 °C).
3. The activation energies for the overall reaction and for the pathway for CO_2 formation decrease slightly with potential, from 32 ± 2 and 39 ± 2 kJ mol^{-1} at 0.6 V to 27 ± 1 and 42 ± 1 kJ mol^{-1} at 0.7 V in 0.1 M solution, respectively. Correspondingly, also the current efficiencies for CO_2 formation decrease with increasing potential, e.g., from 39% (27%) at 0.6 V to 15% (9%) at 0.7 V at 100 °C (80 °C). The decrease in both quantities with potential is associated with a transition in the rate limiting step, from CO_{ad} oxidation at lower potentials to C—C bond breaking (CO_{ad} formation) at higher potential.
4. Contrary to ethanol oxidation, transport effects play only a limited role in acetaldehyde oxidation, since contributions from re-adsorption and further reaction of reactive reaction intermediates are negligible, due to the very low reactivity of acetic acid under present reaction conditions. They only come into play via different compositions of the adlayer, i.e., different coverages of different coexisting adsorbates during reaction in solutions of different reactant (acetaldehyde) concentration.
5. Significant differences between the CO_2 current efficiencies determined in potentiodynamic measurements and under steady-state conditions in potentiostatic measurements at similar potentials are explained by a combination of different effects specific for potentiodynamic measurements: (i) the convolution of potential and time effects in potentiodynamic measurements, which result in different adlayer coverages and compositions in both types of measurements at a given potential and (ii) the oxidation of adsorbed species pre-formed at other (lower) potentials, which leads to lower electron yields per CO_2 molecule formation compared to complete oxidation of acetaldehyde to CO_2. Due to these effects, only the CO_2 current efficiencies determined under steady-state conditions are reliable for quantitative comparison with fuel cell measurements and operation, while the validity of values determined in potentiodynamic measurements is limited to qualitative discussions of the trends.
6. From the linear correlation between $\ln r$ and $1/T$ over the full temperature range in the Arrhenius plots, both for the overall reaction and for the partial reactions (incomplete oxidation to acetic acid and complete oxidation to CO_2), we conclude that the rate limiting reaction steps in the two reaction pathways do not change with temperature over the entire temperature scale.
7. Acetic acid is essentially inactive to further oxidation to CO_2 even at 100 °C under present experimental condition. This goes along with a very high apparent activation energy for this reaction of between 110 and 200 kJ mol^{-1}, depending on the potential, which is much higher than the values for ethanol oxidation or acetaldehyde oxidation under identical reaction conditions.

For practical applications in a direct oxidation fuel cell it is important to note that improvements in the general activity of the acetaldehyde oxidation reaction require a higher activity of the respective catalyst in two reactions, in C—C bond breaking (CO_{ad} formation) and in CO_{ad} oxidation. If only one of these two partial reactions is accelerated, this will lead to rate limitations by the

respective other partial reaction (C—C bond breaking at high potentials, CO_{ad} surface blocking at lower potentials). This explains also the much smaller improvements reached by bimetallic catalysts for ethanol and acetaldehyde oxidation as compared to methanol oxidation.

Acknowledgements

This work was supported by the Federal Ministry of Research and Technology (project 03SF0311C), by the Helmholtz Association (project VH-VI-139) and by the Baden-Württemberg Foundation within the Project 'Portable Mini-Fuel Cells' (grant No. MBZ 20).

References

[1] A. Wieckowski, J. Sobrowski, P. Zelenay, K. Franaszczuk, Electrochim. Acta 26 (1981) 1111.
[2] D.S. Corrigan, E.K. Krauskopf, L.M. Rice, A. Wieckowski, M.J. Weaver, J. Phys. Chem. 92 (1988) 1596.
[3] J.L. Rodríguez, E. Pastor, X.H. Xia, T. Iwasita, Langmuir 16 (2000) 5479.
[4] J. Silva-Chong, E. Méndez, J.L. Rodríguez, M.C. Arévalo, E. Pastor, Electrochim. Acta 47 (2003) 1441.
[5] K.B. Kokoh, F. Hahn, E.M. Belgsir, C. Lamy, A.R. de Andrade, P. Olivi, A.J. Motheo, G. Tremiliosi-Filho, Electrochim. Acta 49 (2004) 2077.
[6] M.J.S. Farias, G.A. Camara, A.A. Tanaka, T. Iwasita, J. Electroanal. Chem. 600 (2007) 236.
[7] C. Lamy, A. Lima, V. Le Rhun, F. Delime, C. Coutanceau, J.-M. Léger, J. Power Sources 105 (2002) 283.
[8] C. Lamy, E.M. Belgsir, in: W. Vielstich, H.A. Gasteiger, A. Lamm (Eds.), Fundamentals and Survey of Systems, vol. 1, Wiley, Chichester, 2003 (Chapter 19).
[9] R. Dillon, S. Srinivasan, A.S. Arico, V. Antonucci, J. Power Sources 127 (2004) 112.
[10] C. Lamy, S. Rousseau, E.M. Belgsir, C. Coutanceau, J.-M. Léger, Electrochim. Acta 49 (2004) 3901.
[11] S. Rousseau, C. Coutanceau, C. Lamy, J.-M. Léger, J. Power Sources 158 (2006) 18.
[12] E. Antolini, J. Power Sources 170 (2007) 1.
[13] F. Cases, E. Morallon, J.L. Vazquez, J.M. Perez, A. Aldaz, J. Electroanal. Chem. 350 (1993) 267.
[14] E. Mendéz, J.L. Rodríguez, M.C. Arévalo, E. Pastor, Langmuir 18 (2002) 763.
[15] H. Zhao, J. Kim, B.E. Koel, Surf. Sci. 538 (2003) 147.
[16] F. Delbecq, F. Vigne, J. Phys. Chem. B 109 (2005) 10797.
[17] H. Wang, Z. Jusys, R.J. Behm, J. Appl. Electrochem. 36 (2006) 1187.
[18] G. Wu, R. Swaidan, G. Cui, J. Power Sources 172 (2007) 180.
[19] S.C.S. Lai, M.T.M. Koper, Faraday Discuss. 140 (2008) 399.
[20] M. Heinen, Z. Jusys, R.J. Behm, J. Phys. Chem. C 114 (2010) 9850.
[21] S. Sun, M. Chojak, M. Heinen, Z. Jusys, R.J. Behm, J. Power Sources 190 (2009) 2.
[22] L.M. Rice, E.K. Krauskopf, A. Wieckowski, J. Electroanal. Chem. 239 (1988) 413.
[23] B. Rasch, T. Iwasita, Electrochim. Acta 35 (1990) 989.
[24] A. Rodes, E. Pastor, T. Iwasita, J. Electroanal. Chem. 376 (1994) 109.
[25] H. Wang, Z. Jusys, R.J. Behm, Fuel Cells 4 (2004) 113.
[26] M.H. Shao, R.R. Adzic, Electrochim. Acta 50 (2005) 2415.
[27] M. Heinen, Z. Jusys, R.J. Behm, in: H.A. Gasteiger, W. Vielstich, H. Yokogawa (Eds.), Handbook of Fuel Cells, vol. 5, John Wiley and Sons, Chichester, 2009 (Chapter 12).
[28] S.C.S. Lai, S.E.F. Kleyn, V. Rosca, M.T.M. Koper, J. Phys. Chem. C 112 (2008) 19080.
[29] T. Iwasita, X. Xia, H.-D. Liess, W. Vielstich, J. Phys. Chem. B 101 (1997) 7542.
[30] E.K. Krauskopf, A. Wieckowski, J. Electroanal. Chem. 271 (1989) 295.
[31] V. Rao, C. Cremers, U. Stimming, L. Cao, S. Sun, S. Yan, G. Sun, Q. Xin, J. Electrochem. Soc. 154 (2007) B1138–B1147.
[32] H. Nonaka, Y. Matsumura, J. Electroanal. Chem. 520 (2002) 101.
[33] J. Wang, S. Wasmus, R.F. Savinell, J. Electrochem. Soc. 142 (1995) 4218.
[34] A.S. Aricò, P. Creti, P.L. Antonucci, V. Antonucci, Electrochem. Solid State Lett. 1 (1998) 66.
[35] D.D. James, P.G. Pickup, Electrochim. Acta 55 (2009) 3824.
[36] J. Fuhrmann, H. Zhao, E. Holzbecher, H. Langmach, M. Chojak, R. Halseid, Z. Jusys, R.J. Behm, Phys. Chem. Chem. Phys. 10 (2008) 3784.
[37] Z. Jusys, R.J. Behm, ECS Trans. 16 (2008) 1243.
[38] M. Chojak Halseid, Z. Jusys, R.J. Behm, J. Phys. Chem. C 114 (2010) 22573.
[39] M. Chojak Halseid, Z. Jusys, R.J. Behm, J. Electroanal. Chem. 664 (2010) 103.
[40] Z. Jusys, J. Kaiser, R.J. Behm, Phys. Chem. Chem. Phys. 3 (2001) 4650.
[41] T.J. Schmidt, H.A. Gasteiger, G.D. Stäb, P.M. Urban, D.M. Kolb, R.J. Behm, J. Electrochem. Soc. 145 (1998) 2354.
[42] H. Wang, Z. Jusys, R.J. Behm, J. Phys. Chem. B 108 (2004) 19413.
[43] J.C. Davies, G. Tsotridis, J. Phys. Chem. C 112 (2008) 3392.
[44] T.H. Madden, E.M. Stuve, J. Electrochem. Soc. 150 (2003) E571.
[45] T. Kawaguchi, W. Sugimoto, Y. Murakami, Y. Takasu, Electrochem. Commun. 6 (2004) 480.
[46] T. Seiler, E.R. Savinova, K.A. Friedrich, U. Stimming, Electrochim. Acta 49 (2004) 3927.
[47] N. Wakabayashi, H. Uchida, M. Watanabe, Electrochem. Solid State Lett. 5 (2002) E62.
[48] E. Herrero, B. Alvarez, J.M. Feliu, S. Blais, Z. Radovic-Hrapovic, G. Jerkiewicz, J. Electroanal. Chem. 567 (2004) 139.
[49] R.J. Behm, Z. Jusys, J. Power Sources 154 (2006) 327.
[50] S. Sen Gupta, J. Datta, J. Electroanal. Chem. 594 (2006) 65.
[51] I. Shimada, Y. Oshima, J. Otomo, J. Electrochem. Soc. 158 (2011) B369.
[52] T. Iwasita, J. Brazil. Chem. Soc. 13 (2002) 401.
[53] H. Wang, Z. Jusys, R.J. Behm, J. Power Sources 154 (2006) 351.
[54] E. Herrero, J.M. Feliu, S. Blais, Z. Radovic-Hrapovic, G. Jerkiewicz, Langmuir 16 (2000) 4779.
[55] A. Schneider, L. Colmenares, Y.E. Seidel, Z. Jusys, B. Wickman, B. Kasemo, R.J. Behm, Phys. Chem. Chem. Phys. 10 (2008) 1931.
[56] Y.E. Seidel, A. Schneider, Z. Jusys, B. Wickman, B. Kasemo, R.J. Behm, Faraday Discuss. 140 (2008) 167.
[57] Y.E. Seidel, A. Schneider, Z. Jusys, B. Wickman, B. Kasemo, R.J. Behm, Langmuir 26 (2010) 3569.
[58] R.B. Kutz, B. Braunschweig, P. Mukherjee, R.L. Behrens, D.D. Dlott, A. Wieckowski, J. Catal. 278 (2011) 181.
[59] C. Liakopoulos, S. Poulopoulos, C. Philippopoulos, Ind. Eng. Chem. Res. 40 (2001) 1476.
[60] N.M. Markovic, T.J. Schmidt, B.N. Grgur, H.A. Gasteiger, R.J. Behm, P.N. Ross, J. Phys. Chem. B 103 (1999) 8568.
[61] Y. Luo, Handbook of Bond Dissociation Energies in Organic Compounds, CRC Press, 2002.
[62] H.F. Wang, Z.P. Liu, J. Am. Chem. Soc. 130 (2008) 10996.
[63] A. Kowal, M. Li, M. Shao, K. Sasaki, M. Vukovic, J. Zhang, N.S. Marinkovic, P. Liu, A.I. Frenkel, R.R. Adzic, Nat. Mater. 8 (2009) 1.
[64] M. Li, A. Kowal, K. Sasaki, N. Marinkovic, D. Su, E. Korach, P. Liu, R.R. Adzic, Electrochim. Acta 55 (2010) 4331.